Dyes and Pigments 174 (2020) 108014

Contents lists available at ScienceDirect

Dyes and Pigments

journal homepage: http://www.elsevier.com/locate/dyepig

Perylene-diimide-based n-type semiconductors with enhanced air and temperature stable photoconductor and transistor properties

Jonathan D. Yuen [a,**,1], Vladimir A. Pozdin [b,1], Ashlyn T. Young [c], Brendan L. Turner [c], Ian D. Giles [a], Jawad Naciri [a], Scott A. Trammell [a], Paul T. Charles [a], David A. Stenger [a], Michael A. Daniele [b,c,*]

[a] Center for Bio/Molecular Science and Engineering, Code 6910, U.S. Naval Research Laboratory, Washington, DC, 20375, USA
[b] Department of Electrical and Computer Engineering, North Carolina State University, Raleigh, NC, 27695, USA
[c] Joint Department of Biomedical Engineering, North Carolina State University and University of North Carolina at Chapel Hill, Raleigh, NC, 27695, USA

ARTICLE INFO

Keywords:
Perylene
n-type
Photoconductor
Field effect transistor
Air stable

ABSTRACT

We report the synthesis and characterization of highly air and temperature stable, solution-processed, n-type organic semiconductors: a perylene-diimide monomer and a perylene-diimide-based pendant polymer. When integrated into a transistor structure, both materials possess pure n-type transport with mobility as high as 10^{-5} $cm^2 V^{-1} s^{-1}$ for the polymer. The organic semiconductors exhibit good photoconductor properties, with photocurrent to dark current ratios of up to 10^3 for the monomer, despite its lower FET mobility. The differences in transistor and photoconductor properties suggest different applications for each material. Both materials can be processed in air, and their transport properties have good air stability, improving with annealing even up to 200 °C in air. It is notable that such air-stable photoconductivity and transport properties have rarely been reported for n-type organic semiconductors before, as most n-type organic semiconductors are not stable in air. Hence, these materials may have potential in a wide range of applications.

1. Introduction

Solution-processible organic semiconductors offer potentially inexpensive active components in large area electronics as complementary circuits (CMOS), field effect transistors (FETs), radio-frequency ID tags, sensors, organic light-emitting diodes (OLEDs), and photovoltaics (OPVs) [1]. Remarkable progress has been achieved for hole-transporting (p-type) polymer semiconductors with mobilities exceeding 35 $cm^2 V^{-1} s^{-1}$ and with good air and thermal stability [2–4] – suitable for the above mentioned applications. In contrast, the development of stable, purely electron transporting (n-type) materials with good transport properties, and even more importantly, good air and thermal stability [5,6] remains a critical need in the field, as stable, high performance n-type semiconductors are essential for the development of organic CMOS integrated circuits and the expansion of electron accepting materials for organic photovoltaics. With current n-type conjugated materials, the formation of free electrons along the conjugated bond results in the geometric distortion of the bond and the formation of an unstable radical charge [7]. Hence, they are typically energetically unfavorable. Fortunately, n-type charge formation can be stabilized via conjugated donor-acceptor interactions, and strong n-type transport behavior has been reported for donor-acceptor type conjugated organic semiconductors [8,9]. However, these donor-acceptor conjugated semiconductors typically have commensurate p-type transport with varying degrees of strength. For many applications, the simultaneous presence of p-type transport may constitute a problem. For FETs, the presence of p-type transport in an n-type transistor will lead to a lack of, or limited range of, an OFF state. For OPVs, p-type transport states in the n-type region of an organic solar cell will serve as hole-traps and exciton-recombination sites, reducing the photo-performance of the device.

Perylene-diimides (PDIs) are highly electron-deficient conjugated structures that can exist stably in ambient environments, enabling their application as dyes [10,11]. This electron-deficiency, together with

* Corresponding author. Department of Electrical and Computer Engineering, North Carolina State University, Raleigh, NC, 27695, USA.
** Corresponding author.
E-mail addresses: jonathan.yuen@nrl.navy.mil (J.D. Yuen), mdaniel6@ncsu.edu (M.A. Daniele).
[1] Authors equally contributed to this work.

https://doi.org/10.1016/j.dyepig.2019.108014
Received 6 March 2018; Received in revised form 31 October 2019; Accepted 1 November 2019
Available online 4 November 2019

strong intermolecular π- π coupling, results in good n-type transport in well-ordered films of suitably deposited variants of PDI molecules, thereby allowing for numerous electronic applications [12–15]. PDI-based pendant polymers have been synthesized *via* "click" [16,17] and nitroxide radical mediated routes [18], and these polymers have exhibited good electron mobility in organic field effect transistors [19]. In particular, PDIs are attractive candidates for n-type active materials for organic solar cells [20]; furthermore, the design space for PDI-based organic electronics has expanded *via* advances in both molecular and device architectures [21–25]. In this paper, we report on the photoconductive properties of a monomer and a pendant polymer, both consisting of PDI with an acrylate-based swallow-tail side-group [26,27]. Devices that we fabricated under ambient conditions showed good transistor and photoconductor performance in air. More significantly, transport properties improved with annealing up to 200 °C in air. The results indicate good environmental stability for these types of PDI organic semiconductors and bodes well for a variety of applications.

2. Materials and methods

2.1. Materials

All starting materials and solvents were obtained from Sigma-Aldrich (St. Louis, MO, USA) and were used as received. The synthesis of the PDI monomer and PDI polymer is described *herein*:

2.1.1. Synthesis of 2-(2-ethylhexyl)-9-(6-hydroxymethyl)anthra[2,1,9-def:6,5,10-d'e'f']diisoquinoline-1,3,8,10(2H,9H)-tetraone (2)

A mixture of 9-(2-ethylhexyl)-1H-isochromeno[6′,5′,4':10,5,6]anthra[2,1,9-def]isoquinoline-1,3,8,10(9H)-tetraone [27] **1** (0.83 g, 1.65 mmol), 6-aminohexan-1-ol (0.23 g, 1.98 mmol) in 5 g of imidazole was stirred for 20 h at 160 °C. After cooling, ethanol and 2 N HCl solutions were added and the mixture was stirred at room temperature for 6 h. The precipitate was collected by filtration, washed with water and dried in a vacuum oven at 130 °C. The final product was obtained as a red solid (0.90 g, 90%). ^{1}H NMR ($CDCl_3$-400 MHz): δ = 8.65 (d, 4H), 8.58 (d, 4H), 4.12 (m, 2H), 4.08 (m, 2H), 3.62 (t, 2H), 2.01 (m, 1H), 1.2–1.8 (m, 16 H), 0.9–0.98 (m, 6H).

2.1.2. Synthesis of 6-(9-(2-ethylhexyl)-1,3,8,10-tetraoxo-3,8,9,10-tetrahydroanthra[2,1,9-def:6,5,10-d'e'f']-diisoquinolin-2(1H)-yl)-hexyl acrylate (3) (PDI monomer)

A mixture of **2** (0.90 g, 1.49 mmol) and anhydrous triethylamine (0.65 mL, 4.68 mmol) in 20 mL of anhydrous dichloromethane was stirred at 0 °C under nitrogen flow. Acryloyl chloride (0.49 mL, 6 mmol) in 5 mL of dichloromethane was subsequently added dropwise while keeping the temperature at 0 °C. The reaction mixture was stirred overnight at room temperature. After diluting with dichloromethane, the organic phase was washed with 10% NaCl solution and dried over $MgSO_4$. The solvent was evaporated under reduced pressure and the crude product was purified by column chromatography on silica gel using (CH_2Cl_2/ethyl acetate 4:1) as the eluents. The final product was obtained as a red solid (0.5 g, 51%). ^{1}H NMR ($CDCl_3$-400 MHz): δ = 8.65 (d, 4H, J = 8 Hz), 8.58 (d, 4H, J = 8 Hz), 6.39 (d, 1H, J = 17 Hz), 6.12 (dd, 1H, J = 17, 10 Hz), 5.79 (d, 1H, J = 10 Hz), 4.06–4.19 (m, 6H), 1.92–2.01 (m, 1H), 1.32–1.80 (m, 16 H), 0.88–0.98 (m, 6H). ^{13}C NMR ($CDCl_3$) δ 165.35, 163.45, 163.04, 134.10, 133.97, 133.05, 131.05, 130.51, 129.00, 128.63, 123.11, 122.79, 64.60, 44.32, 40.50, 37.97, 30.77, 28.72, 28.54, 27.94, 26.96, 25.73, 24.08, 23.10.14.14, 10.80. Anal. Calcd for $C_{41}H_{40}N_2O_6$: C, 74.98; H, 6.14; N, 4.27; O, 14.62. Found: C, 71.88; H, 4.79; N, 3.06; O, 19.88. Impurities are attributed to hygroscopic water adsorption and solvent trapping. Mass Measured: m/z 657.29 $[M+H]^+$; m/z 656.29 $[M]^-$. Mass Calculated: m/z 656.29.

2.1.3. Synthesis of poly(perylene diimide acrylate) (4) (PDI polymer)

A mixture of **3** (0.16 g, 0.24 mmol) and AIBN (1.4 mg, 0.008 mmol) was dissolved in 0.6 mL of 1,2-dichlorobenzene. The reaction mixture was degassed by three freeze/thaw cycles and stirred under nitrogen for 10 h at 70 °C. After cooling down to room temperature, the polymer was purified by precipitation from tetrahydrofuran (THF) solution into acetone. After centrifugation and drying at 50 °C in vacuum oven, pure polymer was obtained in 60% yield (0.096 g). ^{1}H NMR ($CDCl_3$-400 MHz): δ = 8.65–8.58 (m, br, 8H), 4.10–4.23 (m, 4H), 3.90 (m, 2H), 2.01 (m, 1H), 1.2–1.9 (m, 19 H), 0.9–0.98 (m, 6H). ^{13}C NMR ($CDCl_3$) δ 175.85, 163.00, 162.75, 134.10, 133.97, 133.05, 131.05, 129.00, 123.11, 122.79, 64.60, 49.10, 44.32, 40.50, 37.97, 30.77, 28.72, 28.54, 27.94, 26.96, 25.73, 24.19, 24.08, 23.10.14.14, 10.80. IR (cm^{-1}): 2956, 2931, 2860, 1726, 1695, 1652, 1404, 1348, 1250, 1182, 810, 746.

2.2. NMR and chromatography

^{1}H and ^{13}C NMR measurements of polymer and monomer samples in $CDCl_3$ were performed on a Bruker 300 MHz NMR spectrometer. The data were analyzed using Bruker TopSpin NMR version 3.5p17. All column chromatography was performed using Mallinckrodt Chemicals silica grade 62 (60–200 mesh). Analytical thin layer chromatography (TLC) was performed on Merck silica gel 60 F254 plates.

2.3. Gel permeation chromatography

Molecular weight characterization was tested using a Waters 515 HPLC gel permeation chromatography (GPC) system coupled with a Waters 2489 UV/visible detector and a 2414 refractive index detector. The polymer was put into a 1 mg/mL solution in THF and let sit overnight (~12 h) and then filtered through a 0.45 μm GHP membrane filter. Three sets of polystyrene known standards (ranging from MW of 994,000 down to 2320) were run and used for the calibration of the machine. The tests were run at a flowrate of 1.0 mL/min. Molecular weight (Mw) of the polymer was measured to be 653,650 Daltons or close to 1000 repeat units with polydispersity index of 1.14.

2.4. Elemental analysis

Carbon, hydrogen, and nitrogen analysis was analyzed by normal combustion using a PerkinElmer 2400 Elemental Analyzer. This analyzer uses combustion to convert the sample elements to simple gases, i.e., CO_2, H_2O, N_2. Upon entering the analyzer, the sample is combusted in a pure oxygen environment. The product gases are separated under steady state conditions and measured as a function of thermal conductivity. PDI monomer and polymer samples were recrystallized by precipitation from tetrahydrofuran into acetone twice, then from tetrahydrofuran into methanol prior to elemental analysis. Oxygen was analyzed by pyrolysis using a PerkinElmer 2400 Elemental Analyzer, fitted with an oxygen accessory kit to determine oxygen in organic materials. The analyzer uses pyrolysis to convert the oxygen to carbon monoxide. The carbon monoxide is then separated from the other pyrolozates under steady state conditions and measured as a function of thermal conductivity.

2.5. Mass spectrometry

Analysis of monomer (**Compound 3**) was carried out on a high resolution mass spectrometer – the Thermo Fisher Scientific Exactive Plus MS, a benchtop full-scan Orbitrapä mass spectrometer – using Heated Electrospray Ionization (HESI). Sample was dissolved in acetonitrile and analyzed via flow injection into the mass spectrometer at a flow rate of 200 μL/min. The mobile phase was 90% acetonitrile with 0.1% formic acid and 10% water with 0.1% formic acid. The mass spectrometer was operated in positive and negative ion modes.

2.6. Electrochemical measurements

Cyclic voltammetry (CV) measurements of the organic semiconductors, measured against ferrocene, were carried out in dichloromethane on a CH Instruments 1000C potentiostat, with a scan rate of 100 mV s^{-1}. Tetrabutylammonium tetrafluoroborate, 0.1 M, was the supporting electrolyte. Platinum disks were used as the working and counter electrodes, with a Ag disk quasi-reference electrode. Before measurements, the electrodes were cleaned on a velvet disk with a SiC frit of 100 μm diameter, rinsed with acetone and methanol, and then sonicated in deionized water. For each measurement, ferrocene was used as an internal standard, with the HOMO (oxidation potential) of ferrocene set as 4.8 eV.

2.7. Spectroscopic measurements

Absorption spectra of the PDI monomer and PDI polymer in dilute tetrahydrofuran (0.4 mg mL^{-1}) were obtained with a Cary 60 UV–Vis spectrophotometer. PDI monomer and polymer solutions in tetrachloroethane (20 mg mL^{-1}) were drop-cast on a glass slide, dried overnight, and annealed at 150 °C for thin film absorption measurements. Absorbance spectra were measured from λ = 400–700 nm. Photoluminescence spectra of the PDI monomer and the PDI polymer in dilute tetrahydrofuran solution (0.4 mg mL^{-1}) at excitation wavelength λ_{ex} = 485 nm were obtained with an Edinburgh Instruments FLS980 fluorescence spectrometer.

2.8. Computational methods

Calculations were performed using GAUSSIAN 09W software package [28]. Graphical representation and analysis of the calculations were produced using Avogadro and ChemDraw3D software packages. Geometry optimization parameters for the ground electronic states and vibrational frequencies were calculated for comparison to experimental measurements. The electronic properties of monomers were calculated using density functional theory (DFT) method with the three-parameter hybrid exchange functional of Becke and the Lee-Yang-Parr correlation functional (B3LYP) [29,30], and the 6-31G* basis set [31]. Oligomers (n = 2,3,4) were used to represent the polymer in simulations due to computational restrictions.

2.9. Fabrication and characterization of FET devices

Organic field-effect transistors were fabricated in the bottom gate, bottom contact configuration on heavily-doped n-type Si substrates with 200 nm thermally grown silicon dioxide as the gate dielectric layer (Silicon Quest, dry oxide). The device architecture is illustrated in Fig. 1a. The source and drain electrodes were patterned using standard photolithography and were formed on SiO_2 with e-beam evaporation of 5 nm of chromium and 45 nm of gold. Prior to deposition, devices were cleaned in acetone and isopropanol, and dried at 120 °C for 15 min, then exposed for 30 min to UV light in air. The devices were surface treated with decyltriethoxysilane (DTS) for 0.5 h by immersion in a solution containing 30% by volume of DTS in toluene. The devices were then cleaned by rinsing with toluene and dried under nitrogen flow. Polymer films were spin-cast on the passivated substrates at 4,000 RPM in air from a 15 mg mL^{-1} solution in dichloromethane. For spin-coating, PDI solutions of high boiling point solvents, such as tetrachloroethane, could not wet the substrate as this would result no film formation. Samples were then annealed at 150 °C for 10 min in air prior to measurement. FET mobility measurements were performed in air using an Agilent 4550 Semiconductor Parametric Analyzer controlled by a custom LabView program on a Micromanipulator probe station. The devices composed of PDI polymers had channel lengths and widths of 120 μm and 500 μm, respectively. The devices composed of PDI monomers had channel lengths and widths of 30 μm and 1000 μm, respectively, to compensate for their low currents.

2.10. Photoconductivity measurements

The samples used for photoconductivity measurements were planar devices with two bottom contacts. The device architecture is illustrated in Fig. 1b. Glass substrates were cleaned in acetone and isopropanol and dried in an oven at 120 °C. The electrodes were patterned using standard photolithography with e-beam evaporation of 5 nm of chromium and 45 nm of gold. PDI polymer films were drop-cast from a 20 mg mL^{-1} solution in tetrachloroethane from a micropipette calibrated at 5 μL. Films drop-cast with tetrachloroethane resulted in smoother, more uniform films than films drop-cast with dichloromethane. Samples were dried at room temperature overnight. Photoconductivity measurements were performed in air using an Agilent 4550 Semiconductor Parametric Analyzer controlled by a custom LabView program on a probe station with samples annealed at various temperatures. For each temperature, samples were annealed for 10 min in air prior to measurement. To perform photoconductivity measurements, samples were exposed to a halogen double light source (Dolan Jenner Fiber-Lite 180 series, intensity at approx. 30 W m^{-2}) for photocurrent-voltage measurements, and to room-light for dark current-voltage measurements. Room light was used as we found no significant difference between dark and room-light environments. Samples measured had electrode gaps of 30 μm.

2.11. DSC measurements

Differential Scanning Calorimetry (DSC) data were measured on a TA Instruments Q2000 in hermetically sealed aluminum pans. Powder samples were used for measurements (2.6 mg of monomer and 2.7 mg of polymer). The samples were equilibrated at 10 °C and then heated from 10 °C to 250 °C and cooled from 250 °C to 10 °C at a linear ramp rate of 5 °C/min three times.

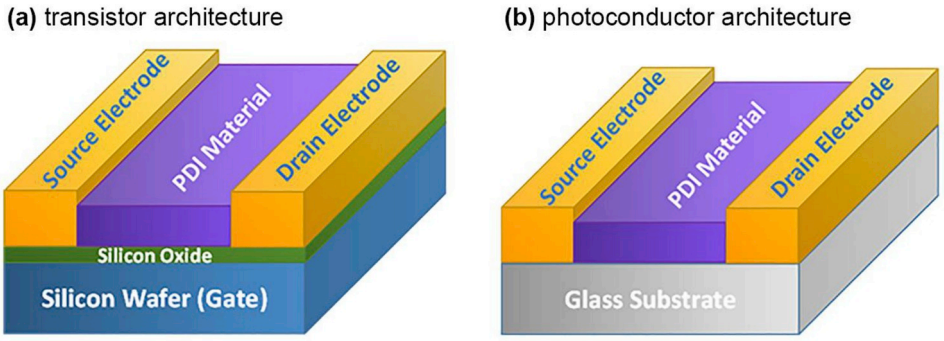

Fig. 1. Diagrammatic descriptions of the device architectures studied, (a) transistor and (b) photoconductor.

2.12. TGA measurements

Thermogravimetric Analysis (TGA) measurements were performed on a TA Instruments Q500. Samples were run from 35 °C to 700 °C at a linear ramp rate of 20 °C·min^{-1} under N_2 purge.

3. Results and discussion

3.1. Synthesis of perylene-diimide monomer and pendant polymer

Synthesis of the PDI monomer and PDI polymer is illustrated in Scheme 1. The synthesis of the starting unsymmetric perylene monoimide mono-anhydride molecule (**1**) was modified from previous report by Mery et al. [27] The synthesis of the PDI monomer and pendant polymer was modified from previous reports by Haberkorn et al. and Kota et al. [32,33] Starting molecule yields were good (≈90%) for compounds **1** and **2**, while moderate yields 50% for hydrolysis into monomer (**3**) and 60% yield for free-radical polymerization (**4**) was expected.

3.2. Electrochemical and optical measurements

Electrochemical and UV–Vis absorption measurements were performed on the PDI monomer and the PDI polymer to determine their energetic properties. For the electrochemical measurements, both the PDI monomer and PDI polymer showed strong reduction peaks and no oxidation peaks when voltage was cycled between −1.6V and 1.4V. Voltage was cycled 10 times per measurement, with little change in peak intensity or position. The results indicate that both PDI-materials are electron-accepting (n-type). The electrochemical data for the PDI materials in solution are shown in Fig. 2a, with data normalized for better comparison; the actual measured data are shown in Fig. S1a in the Supplementary Information. The HOMO energy was determined by calculating the difference between the measured reduction potential (LUMO) and the energy at the experimentally observed electronic absorption band edge. When calibrated against ferrocene, the LUMO level for the PDI monomer is 3.89 eV, while the LUMO level for the PDI polymer is 3.83 eV. To derive the HOMO levels, we used the band gaps based on optical absorbance measurements of thin films as shown in Fig. S2. The bandgap of the PDI monomer is 2.02 eV, while the bandgap of the PDI polymer is 1.97 eV. Hence the HOMO levels are 5.91 eV for the PDI monomer and 5.80 eV for the PDI polymer. Fig. 2b shows the photoluminescence spectra of the PDI monomer and PDI polymer in tetrachloroethane. Both the PDI monomer and PDI polymer display photoluminescence peaks at 530, 570, and 615 nm with $\lambda_{ex} = 485$ nm. Similarity between monomer and polymer optical properties in dilute solution (0.4 mg mL^{-1}) indicates a lack of significant intrachain interaction in the polymer. Solid-state absorption data are shown in Fig. S2. Broader and red shifted absorption of thin films, as compared to solutions, indicate a high degree of aggregation and some π-stacking in both polymer and monomer films.

From the results above, we observe a small difference in electronic properties between the PDI monomer and its PDI polymer counterpart. Thin film absorbance spectrum (Fig. S2) of the polymer is broader as compared to that of the monomer. Additionally, a bathochromic shift is observed for the PDI polymer compared to the monomer, with the absorbance onset at around 629 nm for the polymer compared to that of the monomer at around 615 nm. Bathochromic shifts in organic semiconductors from monomer to polymer typically indicate increased

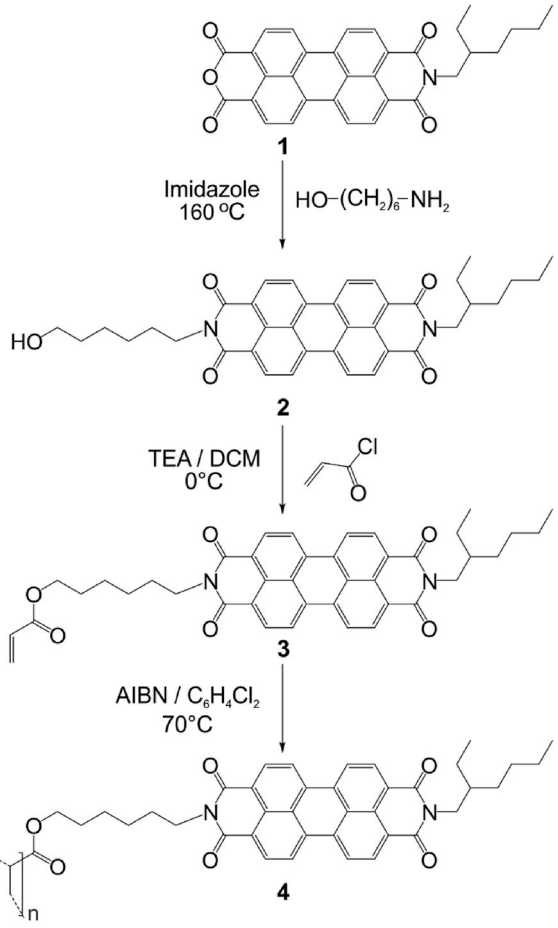

Scheme 1. Synthesis of perylene-diimide-based n-type organic semiconductors.

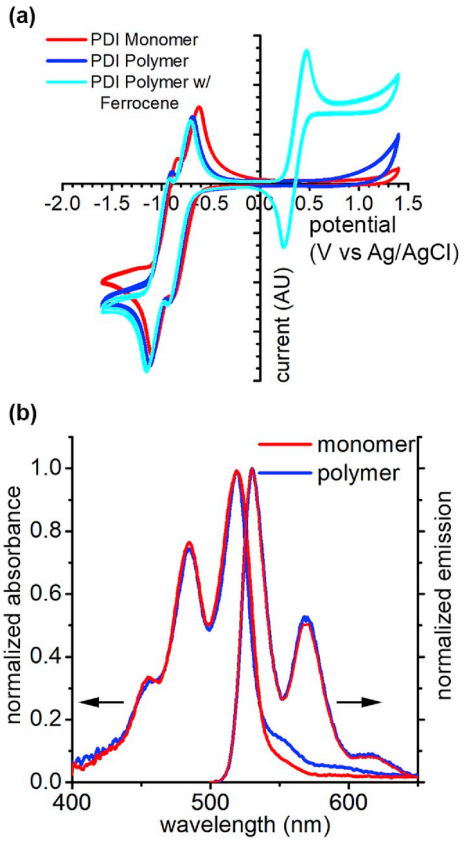

Fig. 2. a) Normalized cyclic voltammograms of the PDI monomer, PDI polymer and PDI polymer with ferrocene in solution. b) UV–Vis absorption and photoluminescence spectra of the PDI monomer and PDI polymer in dilute THF (0.4 mg mL^{-1}).

delocalization of electronic charges, leading to a narrower bandgap and wider spectrum for the polymer. In the presence of a polymeric backbone which enforces alignment of the PDI moieties, overlap of electronic states can occur as the semiconducting moieties come in intimate contact with each other in solid state systems, resulting in higher delocalization of free charges and narrower bandgap [34–37]. We expect that higher delocalization will lead to better transport behavior for the polymer, and therefore differences in photoconductive and transistor behavior between the polymer and monomer.

3.3. Comparison to electronic structure calculations

To corroborate the measured bandgap of the PDI monomer and PDI polymer, electronic structure and vibrational frequencies of the representative materials were calculated with density functional theory (DFT). The corresponding electron density diagrams of HOMO and LUMO are shown in Fig. 3, and the corresponding energies are listed in Table 1. The calculated band gap for the monomer and polymer are 2.53 eV and 2.25 eV, respectively. These results are very similar to experimentally derived values from electrochemical and spectroscopic measurements. A series of oligomers (n = 2,3,4) were used to calculate the PDI polymer properties; however, no significant changes in the HOMO-LUMO and band gap were detected (data not shown). This result suggests that steric hindrance in the PDI polymer backbone precluded the extended de-localization and reduction of the band gap via pendant-pendant interactions along the polymer chain, as supported by the optical measurements in solution.

3.4. Transistor measurements

The field-effect transistor properties of the PDI polymer and PDI monomer were tested to confirm our interpretations above. Fig. 4a and 4b shows the transfer curves, compared against gate current, of typical PDI polymer and monomer devices, respectively; while Fig. 4c and 4d shows the output curves of the polymer and monomer, respectively. The devices were previously annealed at 150 °C in air, since as-cast samples for both materials did not have significant transistor properties. Improvement in n-type transport indicates that both the PDI polymer and monomer are air and temperature stable. Comparing the transfer and output behaviors of the two materials, we observe that the transistor current of the monomer was lower than that of the polymer. This lower current occurred despite the monomer device having the shorter channel length and larger channel width. For the transfer curves, significant current is observed in the negative voltage regime. This characteristic is primarily due to gate leakage current rather than the presence of a hole current. However, in the positive gate voltage regime, *i.e.* electron transport, the source-drain current exceeds the gate leakage current by at least an order of magnitude for the polymer, with a smaller difference between source-drain and leakage currents for the monomer. We believe that the leakage current is the cause of the distortion in output current observed at lower source-drain and gate voltages for the monomer device. The transport behaviors of both materials indicate that they are electron transporting semiconductors as indicated by electrochemical measurements, similar to other PDI materials [17,38,39], with a mobility of 1.4×10^{-5} $cm^2 \cdot V^{-1}s^{-1}$ for the polymer and 1.3×10^{-7} $cm^2 \cdot V^{-1}s^{-1}$ for the monomer, calculated in the high gate and source-drain voltages regime.

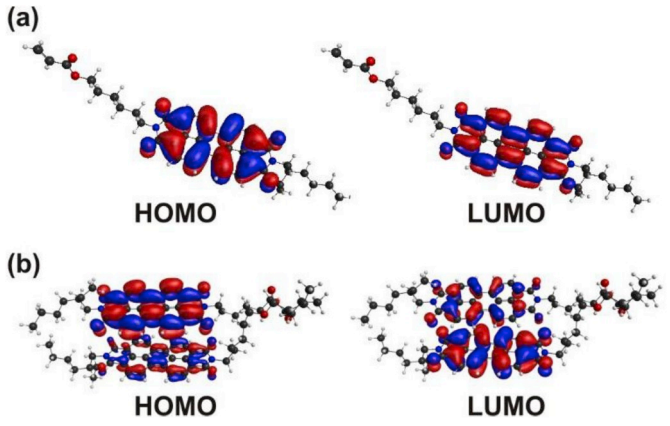

Fig. 3. The density diagram plots of the frontier molecular orbitals of PDI monomer (a) and polymer (b).

Table 1
Summary of calculated and observed energy level parameters of PDI monomer and PDI polymer.

	Energy (eV)					
	E_{HOMO}[a]	E_{LUMO}[a]	E_g[b]	E_{HOMO}[c]	E_{LUMO}[d]	E_g[e]
PDI Monomer	−5.90	−3.37	2.53	−5.91	−3.89	2.02
PDI Polymer	−5.87	−3.62	2.25	−5.80	−3.83	1.97

[a] Determined from DFT simulations.
[b] Determined as the difference between LUMO and HOMO levels, $|E_{LUMO}-E_{HOMO}|$.
[c] Calculated by subtracting the optical bandgap energy from the LUMO level.
[d] Determined from CV based on the reduction onset, corrected by the ferrocene/ferrocenium redox couple potential taken as −4.80 eV.
[e] Determined from the onset of absorption of thin films (Fig. S2).

The transport properties derived from transistor measurements of the PDI polymer and monomer corroborate well with the prior results from the UV–Vis and electrochemical measurements. The poorer transport properties of the monomer compared to polymer suggests: 1) the solution casting of the PDI monomer resulted in an amorphous film in which electronic overlap between individual semiconducting units was poor, and 2) the charge transfer between the units was constrained. In comparison, forcing the individual PDI moieties to align against each other via an intervening polymer backbone enabled better electronic overlap and hence better charge transfer. Thus, the PDI polymer has significantly better mobility compared to the weak transistor behavior observed in the PDI monomer. We therefore conclude that, for solution processing of transistor devices containing PDI-based materials, it is far better to use a pendant polymer consisting of PDI moieties rather than simply casting the PDI monomer, since the alignment between the PDI semiconducting units can be better retained *via* the intervening polymer backbone. We note, however, that both materials are suitable for applications that require temperature and air stability, since transistor behavior improves with annealing up to 200 °C. This finding is significant, since most organic field-effect transistors show degradation in performance when subjected to high temperatures in ambient conditions.

3.5. Photoconductivity measurements

For photocurrent and dark current measurements, current-voltage sweeps from −40V to 40 V were performed on drop-cast films of the two materials. Dark current measurements were performed in room light, and photocurrent measurements, under intense illumination from a halogen light source. Fig. 5a and b shows typical current-voltage (IV) measurements for the PDI polymer and PDI monomer, respectively, with both devices annealed at 150 °C. The IV measurements are plotted in log form to distinguish the photocurrent and dark current more clearly. Linear IV curves are provided in the SI (Fig. S3a and **S3b)**. We observe from the measurements that the polymer shows higher photocurrent and dark current than the monomer, with photocurrents in the tens of nanoamperes for the polymer versus single-digit nanoamperes for the monomer. The higher currents observed for the polymer correlates with our previously reported electrochemical, optical and transistor observations, which indicate higher delocalization of electronic charges in

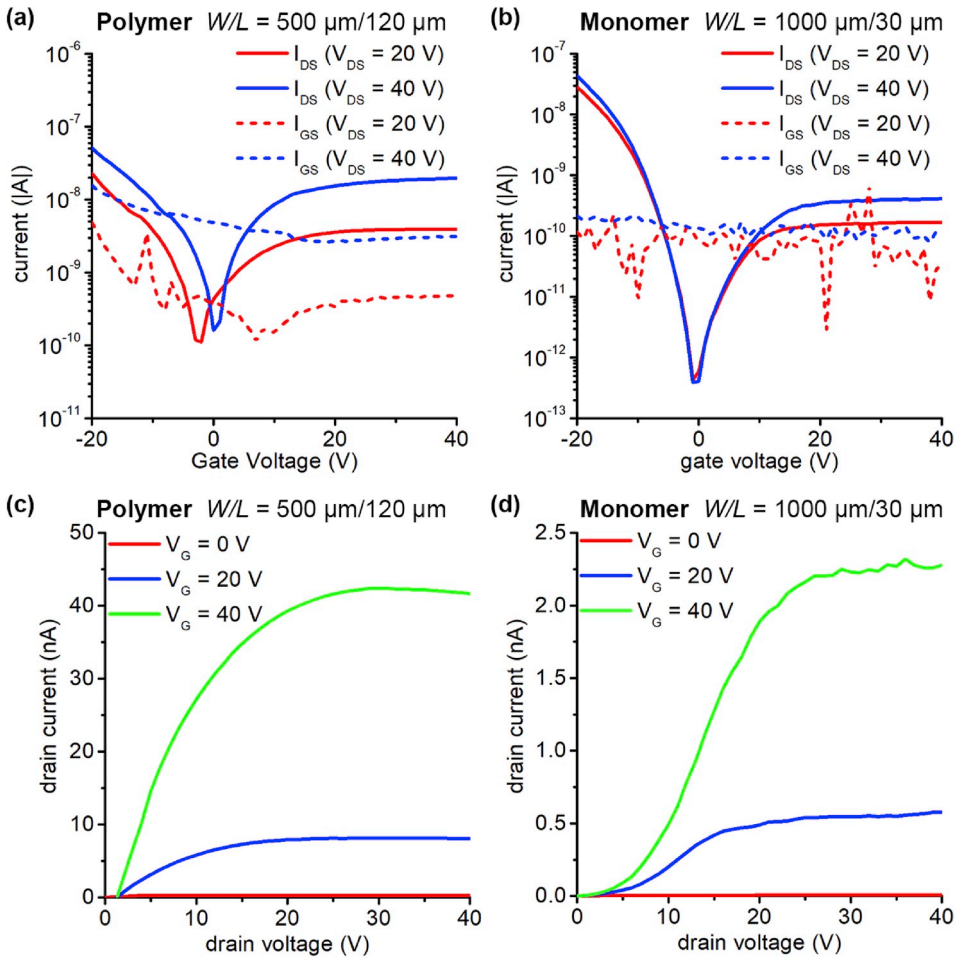

Fig. 4. Transistor transfer curves for (a) PDI polymer and (b) PDI monomer. Transistor output curves for the (c) PDI polymer and (d) PDI monomer. All devices were previously annealed at 150 °C in air.

polymer thin films, and therefore higher mobility of the charges, either photo-generated or injected.

Fig. 5c shows the photocurrents of multiple devices from each material at an applied voltage of 40V. The devices have been annealed and tested over a large temperature range, with the highest annealing temperature at 200 °C. All annealing treatments were performed in air. We observe that the photocurrents for both the polymer and the monomer remained air and thermally stable up to 200 °C. For the polymer, change in photocurrent with annealing was not significant, while the monomer photocurrent increased by over an order of magnitude with annealing. Nonetheless, the monomer photocurrent remained consistently lower than that of the polymer, in agreement with our hypothesis that the polymer would have better transport properties than the monomer. Fig. 5d shows the photocurrent to dark current ratios (I_{photo}/I_{dark}) of the devices over the same annealing range. We observe that the ratio for non-annealed monomer devices was higher, averaging approximately 10^3 compared to 10^2 for polymer devices. At the same time, polymer photocurrent was over an order of magnitude higher than those of monomer devices, indicating large difference in dark currents for non-annealed devices. It is also interesting to note that as annealing temperature increased, the I_{photo}/I_{dark} ratios of the PDI monomer and the PDI polymer approached parity. The results indicate that the dark currents in all devices increased significantly, especially for the monomer. A comparison of the dark currents is provided in the Supporting Information (Fig. S3c).

As previously mentioned, the formation of PDI moieties into a pendant polymer results in the alignment of individual PDI units and higher charge transport. Improved alignment explains the overall higher photocurrent and dark current of the polymer as compared to the monomer. Nonetheless, the difference in $I_{photo}/I_{dark\ ratios}$ between the polymer and monomer for non-annealed samples is striking since both types of current should be dependent on intrinsic mobility and is not photo-dependent. Additionally, the polymer backbone does not significantly affect the conjugation of PDI moieties, so there should not be a significant difference in photo-generation rate [40].

This ratio difference can be understood by the expected presence of more charge trapping sites in the monomer, especially given its amorphous nature. Charge trapping sites impede dark currents which become injection-limited and therefore low in charge density. In contrast, there is a higher concentration of photo-generated charges due to the high quantum efficiency of PDI [41–43]. A small portion of this large photo-generated charge fills the charge trapping sites, so the remaining photocurrents flow more easily as compared to the dark currents which get trapped. In the case of the polymer, the lower concentration of charge trapping sites means higher intrinsic charge transport, and higher dark current due to lower losses caused by charge trapping. This can also be observed in the behavior of the dark current for the PDI monomer (Fig. S3c). The dark current for the PDI monomer increased by more than three orders of magnitude with annealing. In comparison, the PDI polymer only increased by one order of magnitude with annealing. The annealing process induces more ordering in the monomer compared to the polymer, resulting in higher passivation of charge trapping sites [44–47]. Consequently, annealing at higher temperatures, results in the parity between dark current ratios of PDI monomer and PDI polymer. While the PDI monomer suffers from lower current due to its disordered nature, the same disorder, however, results in lower dark currents while

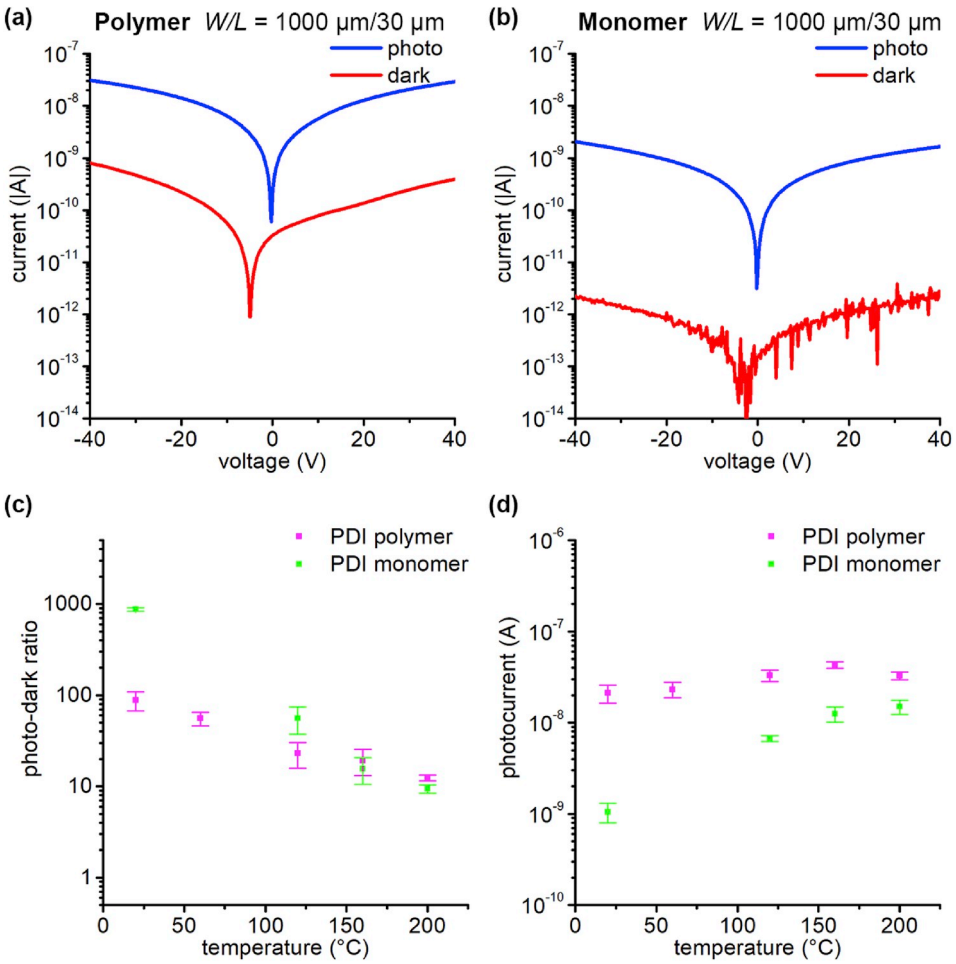

Fig. 5. Typical current-voltage (IV) plots of (a) PDI monomer and (b) PDI polymer measured under light and dark conditions, plot in logarithmic form. (c) Comparison of the photocurrent of the polymer and the monomer annealed at different temperatures from 25 to 200 °C. (d) Comparison of the photocurrent to dark current ratio of the polymer and monomer at different temperatures from 25 to 200 °C.

not strongly affecting the photocurrents, resulting in better photo-responsivity of PDI monomer-based devices.

Charge trapping appears to play a large role in PDI monomer and PDI polymer device performances, and as such, atomic force microscopy is only presented in the Supporting Information to keep the reader from drawing erroneous conclusions. Electric Force Microscopy has demonstrated that charge trapping is not correlated to the surface topography of organic thin films [48]. In fact, the nature of charge trapping sites is not well understood even for a model organic semiconductor, such as pentacene [49]. While AFM topography shows some improvement in film ordering with annealing, no correlation between PDI monomer and PDI polymer charge trapping can be made from AFM.

4. Conclusion

In conclusion, we have synthesized two PDI-based materials–a monomer and a pendant polymer. Both materials are solution-processible, have n-type transistor properties and are stable up to 200 °C in air (with additional TGA and DSC data available in ESI). We show through a series of analyses—UV-Vis, electrochemical, photoconductivity and transistor measurements on solution processed films of both materials—that the transport properties of the PDI polymer are better than those of the monomer. We attribute this to the presence of the backbone of the pendant polymer which enforces a certain degree of alignment of PDI moieties with respect to each other, thereby facilitating electronic overlap between the units, as well as better intermolecular charge transport. In comparison, PDI monomer forms a disordered film with little intermolecular alignment, resulting in the formation of more charge trapping sites. The photoconductive properties, in contrast, are stronger for the PDI monomer, as compared to its polymer counterpart. This can be explained by the higher concentration of trap sites in the monomer which reduces the dark current and thereby increases the I_{photo}/I_{dark} ratio. Overall, our results show that solution-processed, air-and-temperature stable PDI-based materials can be used for diverse applications, such as photoconductors or transistors. However, to maximize the potential of PDI-based devices, it is advisable that we carefully choose between the polymer and monomer for their respective strengths in transistor and photoconductive behavior.

Declaration of competing interest

The authors declare that they have no known competing financial interests or personal relationships that could have appeared to influence the work reported in this paper.

Acknowledgements

This work was funded by the Naval Research Laboratory (NRL) and Office of Naval Research (ONR) 6.1 work unit MA041–06–41–9899 and the Advanced Self-Powered Systems of Integrated Sensors and Technologies (ASSIST), a Nano-Systems Engineering Research Center funded by the National Science Foundation (EEC1160483). All high resolution

mass spectrometry measurements were made in the Molecular Education, Technology, and Research Innovation Center (METRIC) at NC State University. The UV–Vis and PL measurements were performed in the NCSU Chemistry IMAKS lab, Director – Dr. E. O. Danilov. Authors would like to thank Tucker McFarlane and Professor Stephen H. Foulger at Clemson University for the acquisition of the GPC measurement. J.Y. contributed to this work through the American Society for Engineering Education Postdoctoral Fellowship (ASEE). The views are those of the authors and do not represent the opinion or policy of the US Navy or Department of Defense.

Appendix A. Supplementary data

Supplementary data to this article can be found online at https://doi.org/10.1016/j.dyepig.2019.108014.

References

[1] Gamota D. Printed organic and molecular electronics. Boston: Kluwer Academic Publishers; 2004. p. 695. p xxiii.
[2] Liu XF, Hsu BBY, Sun YM, Mai CK, Heeger AJ, Bazan GC. High thermal stability solution-processable narrow-band gap molecular semiconductors. J Am Chem Soc 2014;136(46):16144–7.
[3] Luo C, Kyaw AKK, Perez LA, Patel S, Wang M, Grimm B, Bazan GC, Kramer EJ, Heeger AJ. General strategy for self-assembly of highly oriented nanocrystalline semiconducting polymers with high mobility. Nano Lett 2014;14(5):2764–71.
[4] Kim R, Amegadze PSK, Kang I, Yun HJ, Noh YY, Kwon SK, Kim YH. High-mobility air-stable naphthalene diimide-based copolymer containing extended pi-conjugation for n-channel organic field effect transistors. Adv Funct Mater 2013;23(46):5719–27.
[5] Kuznetsova LI, Piryazev AA, Anokhin DV, Mumyatov AV, Susarova DK, Ivanov DA, Troshin PA. Disubstituted perylene diimides in organic field-effect transistors: effect of the alkyl side chains and thermal annealing on the device performance. Org Electron 2018;58:257–62.
[6] Zschieschang U, Amsharov K, Jansen M, Kern K, Klauk H, Weitz RT. Separating the impact of oxygen and water on the long-term stability of n-channel perylene diimide thin-film transistors. Org Electron 2015;26:340–4.
[7] Yuen JD, Wang MF, Fan J, Sheberla D, Kemei M, Banerji N, Scarongella M, Valouch S, Pho T, Kumar R, Chesnut EC, Bendikov M, Wudl F. Importance of unpaired electrons in organic electronics. J Polym Sci, Polym Chem Ed 2015;53(2):287–93.
[8] Zhao Y, Guo YL, Liu YQ. 25th anniversary article: recent advances in n-type and ambipolar organic field-effect transistors. Adv Mater 2013;25(38):5372–91.
[9] Gao XK, Hu YB. Development of n-type organic semiconductors for thin film transistors: a viewpoint of molecular design. J Mater Chem C 2014;2(17):3099–117.
[10] Greene M. High performance pigments. second ed. Weinheim: Wiley-VCH; 2009. p. 538.
[11] Spillmann CM, Naciri J, Anderson GP, Chen MS, Ratna BR. Spectral tuning of organic nanocolloids by controlled molecular interactions. ACS Nano 2009;3(10):3214–20.
[12] Weitz RT, Amsharov K, Zschieschang U, Villas EB, Goswami DK, Burghard M, Dosch H, Jansen M, Kern K, Klauk H. Organic n-channel transistors based on core-cyanated perylene carboxylic diimide derivatives. J Am Chem Soc 2008;130(14):4637–45.
[13] Zhan XW, Facchetti A, Barlow S, Marks TJ, Ratner MA, Wasielewski MR, Marder SR. Rylene and related diimides for organic electronics. Adv Mater 2011;23(2):268–84.
[14] Liu ZT, Wu Y, Zhang Q, Gao X. Non-fullerene small molecule acceptors based on perylene diimides. J Mater Chem A 2016;4(45):17604–22.
[15] McAfee SM, Dayneko SV, Josse P, Blanchard P, Cabanetos C, Welch GC. Simply complex: the efficient synthesis of an intricate molecular acceptor for high-performance air-processed and air-tested fullerene-free organic solar cells. Chem Mater 2017;29(3):1309–14.
[16] Lang AS, Thelakkat M. Modular synthesis of poly(perylene bisimides) using click chemistry: a comparative study. Polym Chem-Uk 2011;2(10):2213–21.
[17] Lang AS, Muth MA, Heinrich CD, Carassco-Orozco M, Thelakkat M. Pendant perylene polymers with high electron mobility. J Polym Sci, Polym Phys Ed 2013;51(20):1480–6.
[18] Lang AS, Neubig A, Sommer M, Thelakkat M. NMRP versus "click" chemistry for the synthesis of semiconductor polymers carrying pendant perylene bisimides. Macromolecules 2010;43(17):7001–10.
[19] Huttner S, Sommer M, Thelakkat M. n-type organic field effect transistors from perylene bisimide block copolymers and homopolymers. Appl Phys Lett 2008;92(9).
[20] Kozma E, Catellani M. Perylene diimides based materials for organic solar cells. Dyes Pigments 2013;98(1):160–79.
[21] Liu M, Yang J, Yin YL, Zhang Y, Zhou EJ, Guo FY, Zhao LC. Novel perylene diimide-based polymers with electron-deficient segments as the comonomer for efficient all-polymer solar cells. J Mater Chem A 2018;6(2):414–22.
[22] Meena S, Mohammad T, Dutta V, Jacob J. Design and synthesis of N-substituted perylene diimide based low band gap polymers for organic solar cell applications. RSC Adv 2018;8(53):30468–80.
[23] Liu XC, Yin QW, Hu ZC, Wang ZF, Huang F, Cao Y. Perylene diimide based isomeric conjugated polymers as efficient electron acceptors for all-polymer solar cells. Chin J Polym Sci 2019;37(1):18–27.
[24] Lenaerts R, Cardeynaels T, Sudakov I, Kesters J, Verstappen P, Manca J, Champagne B, Lutsen L, Vanderzande D, Vandewal K, Goovaerts E, Maes W. All-polymer solar cells based on photostable bis(perylene diimide) acceptor polymers. Sol Energy Mater Sol Cells 2019;196:178–84.
[25] Liu Z, Du Z, Wang X, Zhu D, Chunming Y, Yang W, Qu X, Bao X, Yang R. Simple perylene diimide based polymer acceptor with tuned aggregation for efficient all-polymer solar cells. Dyes Pigments 2019:170.
[26] Wicklein A, Lang A, Muth M, Thelakkat M. Swallow-tail substituted liquid crystalline perylene bisimides: synthesis and thermotropic properties. J Am Chem Soc 2009;131(40):14442–53.
[27] Schwartz PO, Biniek L, Zaborova E, Heinrich B, Brinkrnann M, Leclerc N, Mery S. Perylenediimide-based donor-acceptor Dyads and triads: impact of molecular architecture on self-assembling properties. J Am Chem Soc 2014;136(16):5981–92.
[28] Frisch MJ, Trucks GW, Schlegel HB, Scuseria GE, Robb MA, Cheeseman JR, Scalmani G, Barone V, Mennucci B, Petersson GA, Nakatsuji H, Caricato M, Li X, Hratchian HP, Izmaylov AF, Bloino J, Zheng G, Sonnenberg JL, Hada M, Ehara M, Toyota K, Fukuda R, Hasegawa J, Ishida M, Nakajima T, Honda Y, Kitao O, Nakai H, Vreven T, Montgomery Jr JA, Peralta JE, Ogliaro F, Bearpark MJ, Heyd J, Brothers EN, Kudin KN, Staroverov VN, Kobayashi R, Normand J, Raghavachari K, Rendell AP, Burant JC, Iyengar SS, Tomasi J, Cossi M, Rega N, Millam NJ, Klene M, Knox JE, Cross JB, Bakken V, Adamo C, Jaramillo J, Gomperts R, Stratmann RE, Yazyev O, Austin AJ, Cammi R, Pomelli C, Ochterski JW, Martin RL, Morokuma K, Zakrzewski VG, Voth GA, Salvador P, Dannenberg JJ, Dapprich S, Daniels AD, Farkas Ö, Foresman JB, Ortiz JV, Cioslowski J, Fox DJ. Gaussian 09. Wallingford, CT, USA: Gaussian, Inc.; 2009.
[29] Becke AD. Density-functional thermochemistry .3. The role of exact exchange. J Chem Phys 1993;98(7):5648–52.
[30] Lee CT, Yang WT, Parr RG. Development of the colle-salvetti correlation-energy formula into a functional of the electron-density. Phys Rev B 1988;37(2):785–9.
[31] Hehre WJ, Ditchfield R, Pople JA. Self-consistent molecular-orbital methods .12. Further extensions of Gaussian-type basis sets for use in molecular-orbital studies of organic-molecules. J Chem Phys 1972;56(5):2257–61.
[32] Haberkorn N, Kim S, Kim KS, Sommer M, Thelakkat M, Sohn BH, Theato P. Template-assisted fabrication of highly ordered interpenetrating polymeric donor/acceptor nanostructures for photovoltaic applications. Macromol Chem Phys 2011;212(19):2142–50.
[33] Kota R, Samudrala R, Mattern DL. Synthesis of donor-sigma-perylenebisimide-acceptor molecules having PEG swallowtails and sulfur anchors. J Org Chem 2012;77(21):9641–51.
[34] Tauber MJ, Kelley RF, Giaimo JM, Rybtchinski B, Wasielewski MR. Electron hopping in pi-stacked covalent and self-assembled perylene diimides observed by ENDOR spectroscopy. J Am Chem Soc 2006;128(6):1782–3.
[35] Che YK, Datar A, Yang XM, Naddo T, Zhao JC, Zang L. Enhancing one-dimensional charge transport through intermolecular pi-electron delocalization: conductivity improvement for organic nanobelts. J Am Chem Soc 2007;129(20):6354–+.
[36] Lin LL, Geng H, Shuai ZG, Luo Y. Theoretical insights into the charge transport in perylene diimides based n-type organic semiconductors. Org Electron 2012;13(11):2763–72.
[37] Ferlauto L, Liscio F, Orgiu E, Masciocchi N, Guagliardi A, Biscarini F, Samori P, Milita S. Enhancing the charge transport in solution-processed perylene di-imide transistors via thermal annealing of metastable disordered films. Adv Funct Mater 2014;24(35):5503–10.
[38] Muth MA, Carrasco-Orozco M, Thelakkat M. Liquid-Crystalline perylene diester polymers with tunable charge-carrier mobility. Adv Funct Mater 2011;21(23):4510–8.
[39] Muth MA, Gupta G, Wicklein A, Carrasco-Orozco M, Thurn-Albrecht T, Thelakkat M. Crystalline vs liquid crystalline perylene bisimides: improved electron mobility via substituent alteration. J Phys Chem C 2014;118(1):92–102.
[40] Kim JY, Chung IJ, Kim YC, Yu JW. Mobility of electrons and holes in a liquid crystalline perylene diimide thin film with time of flight technique. Chem Phys Lett 2004;398(4–6):367–71.
[41] Pasaogullari N, Icil H, Demuth M. Symmetrical and unsymmetrical perylene diimides: their synthesis, photophysical and electrochemical properties. Dyes Pigments 2006;69(3):118–27.
[42] Huang C, Barlow S, Marder SR. Perylene-3,4,9,10-tetracarboxylic acid diimides: synthesis, physical properties, and use in organic electronics. J Org Chem 2011;76(8):2386–407.
[43] Sung J, Kim P, Fimmel B, Wurthner F, Kim D. Direct observation of ultrafast coherent exciton dynamics in helical pi-stacks of self-assembled perylene bisimides. Nat Commun 2015;6.
[44] Fu YY, Yang QQ, Deng YF, Jiang W, Wang ZH, Geng YH, Xie ZY. Suppressed charge recombination in polymer solar cells based on perylene diimide derivative acceptors via solvent vapor annealing. Org Electron 2015;18:24–31.
[45] Kim BJ, Yu H, Oh JH, Kang MS, Cho JH. Electrical transport through single nanowires of dialkyl perylene diimide. J Phys Chem C 2013;117(20):10743–9.
[46] Kim I, Jabbour GE. Effect of annealing on bulk heterojunction organic solar cells based on copper phthalocyanine and perylene derivative. Synth Met 2012;162(1–2):102–6.
[47] Chesterfield RJ, McKeen JC, Newman CR, Ewbank PC, da Silva DA, Bredas JL, Miller LL, Mann KR, Frisbie CD. Organic thin film transistors based on N-alkyl

perylene diimides: charge transport kinetics as a function of gate voltage and temperature. J Phys Chem B 2004;108(50):19281–92.

[48] Smieska LM, Li Z, Ley D, Braunschweig AB, Marohn JA. Trap-clearing spectroscopy in perylene diimide derivatives. Chem Mater 2016;28(3):813–20.

[49] Smieska LM, Pozdin VA, Luria JL, Hennig RG, Hines MA, Lewis CA, Marohn JA. Following chemical charge trapping in pentacene thin films by selective impurity doping and wavelength-resolved electric force microscopy. Adv Funct Mater 2012; 22(24):5096–106.